

Contactless Pulsed and Continuous Microdroplet Release Using Photothermal Liquid Crystals

*Pinar Beyazkilic, Samet Akcimen, Caglar Elbuken, Bülend Ortaç, Shengqiang Cai, and Emre Bukusoglu**

P. Beyazkilic, E. Bukusoglu

Department of Chemical Engineering

Middle East Technical University

Dumlupinar Bulvari No:1 Cankaya, Ankara 06800, Turkey

E-mail: emrebuk@metu.edu.tr

S. Akcimen, B. Ortaç, C. Elbuken

Institute of Materials Science Nanotechnology

National Nanotechnology Research Center (UNAM)

Bilkent University

Ankara 06800, Turkey

C. Elbuken

Faculty of Biochemistry and Molecular Medicine, Faculty of Medicine

University of Oulu

Oulu 90014, Finland

S. Cai

Department of Mechanical and Aerospace Engineering

Materials Science and Engineering Program

University of California, San Diego

La Jolla, California 92093, United States

Targeted, on-demand delivery has been of interest using materials responsive to environmental stimuli such as heat, moisture, chemical and light. Herein, we present a delivery technique based on precise release of aqueous microdroplets from a liquid crystal (LC) medium based on contactless stimulation. A nematic LC was doped with a photothermal dye that produces heat under excitation by near IR (NIR) light. The heat is used to overcome the elastic strains in LC phase which promotes the release of initially entrapped water droplets to the neighboring aqueous solution. Designing the geometry of LC-based emulsions and tuning the light intensity and position provides the manipulation of the release in two distinct modes defined as pulsed and continuous. In pulsed-mode, water droplets are released transiently from the water-in-LC emulsion filled in a mini-well to the aqueous phase based on sweeping by the moving isotropic-nematic (I-N) phase boundary controlled by NIR exposure. In continuous-mode, water droplets are ejected continuously from a droplet-shaped water-in-LC emulsion, due to a heating-induced internal flow and shear controlled by NIR light intensity. The remotely controlled droplet release was used for the on-demand dosing of dopamine and its oxidizing reagent from isolated reservoirs to obtain *in situ* reaction signal for a hydrogen peroxide assay. A new dual-mode release system developed with photothermal LCs holds potential in drug release, controlled mixing, and photothermal therapy.

Keywords: *photothermal heating, liquid crystals, drug delivery, droplet release, NIR light*

1. Introduction

Controlled release of substances is highly desirable due to the side effects arising from high dosing and uptake rates.^[1-3] Stimuli-responsive systems have been developed, which enable the agents to be released on-demand by environmental stimulations such as light, heat, or pH.^[4-8] Most of such systems have been designed with gatekeeper mechanisms made from soft materials (e.g. polymers, lipid-bilayers among the others) which expel the agents at the specific target sites through melting or degradation processes triggered by external stimuli.^[9-14] However, once opened, the “gates” cannot be recovered to stop the release, therefore, there is need for the systems with precise control of phase change that enables a reversible start-stop release mechanism.

Liquid crystals (LCs) are an emerging class of materials that found applications in diverse fields beyond display devices including optical biosensors, actuators, and liquid manipulation owing to the unique structural and optical properties such as elastic anisotropy arising from molecular orientation, reversible phase change, and birefringence.^[15-23] LCs can flow and exhibit mesoscale ordering. They can be designed to switch from anisotropic (ordered) to isotropic state under various stimuli including electric field, heat, and solvent.^[24,25] A recent concept has been reported describing the release of droplets from thermotropic nematic LCs.^[26] Specifically, during phase transition, the boundary between isotropic phase and nematic LC phase (I-N phase boundary) drags the dispersed, micrometer-scale droplets towards the aqueous phase boundary as cargo expelled to the external aqueous solution. The transition from LC to isotropic phase was achieved by contact heating. In another approaches, droplets were released by applying chemical stimuli or by bacterial motion-induced shearing on the LC-aqueous phase interfaces.^[26] However, contactless stimulation of such release systems offers unique features in targeted delivery applications such as ease-of-handling, remote controllability, rapid and repetitive on/off control.

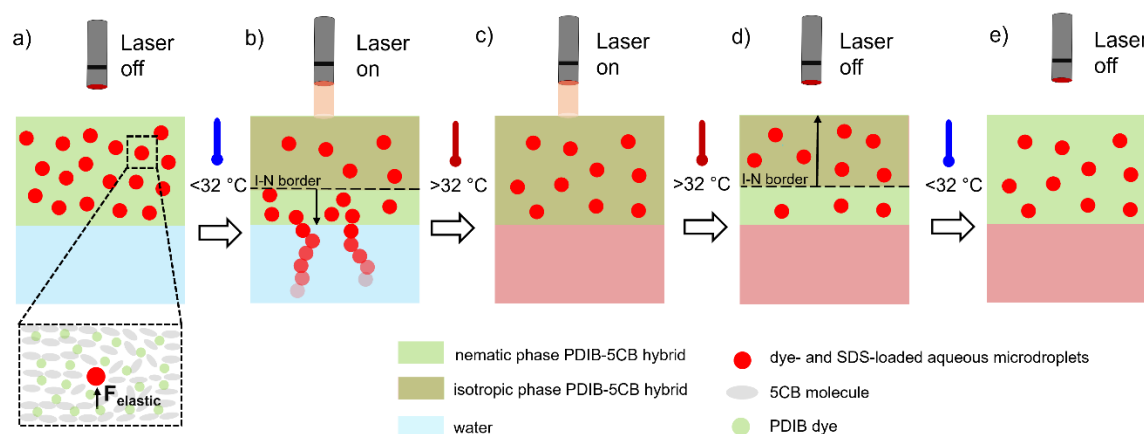
LCs were previously hybridized with fluorescent dyes,^[27-29] azobenzene molecules,^[30-32] gold nanoparticles,^[33,34] and magnetic nanoparticles^[35,36] to design responsive platforms against noncontact electromagnetic sources including UV light, NIR light or magnetic field. NIR light presents particular advantages that include localized exposure, high penetration depth, and low power intensity, which hold significant importance in biomedical fields.^[37] Furthermore, NIR light is converted to heat when absorbed by photothermal agents, therefore it has been extensively used in various heat-mediated applications ranging from photothermal therapy and imaging to actuators and soft robotics.^[38-43] Release of microdroplets which was previously accomplished by applying contact heating or chemical stimuli on the LCs, lacks the spatial

control since heat and chemicals diffuse over the entire LC-aqueous phase interfaces.^[26] In addition, triggering effect induced by chemicals take time to cease. Light-induced release on the other hand, offers spatiotemporal precision with localized excitation as well as the prompt removal of the excitation.

Herein we introduce a microdroplet release method based on NIR excitation using photothermal dye-doped nematic LC. Local excitation combined with rapidly adjustable heating rate and precise on/off control provided by using light, realized a more localized heating and spatiotemporally controlled release. 4-cyano-4'-pentylbiphenyl (5CB); a generic, thermotropic LC, was physically hybridized with N,N,N',N'-tetrakis(p-disobutylaminophenyl)-p-phenylenediimmonium bis(oxalato)borate (PDIB) dye by a solvent-aided mixing. LC-based release system was prepared by emulsification of aqueous (dye-loaded) cargo droplets into photothermal dye-hybridized LC, followed by casting the emulsion on an aqueous phase. Microdroplet release was accomplished remotely by illuminating a NIR laser on the LC surface which generates heat through the photothermal process of the PDIB dye. LC transitioned to isotropic phase due to the photothermal heating and water droplets in the nematic phase were released to the aqueous solution in a pulsed fashion due to the advancing I-N phase boundary. A next release pulse occurred after consecutive laser-off and -on actions. The total released mass was controlled at the microgram level by the number of repeated heating-cooling cycles. Adjustable laser beam spot size and LC dimension provided a precise setting of the released mass in a single pulse. We also serendipitously obtained a novel continuous mode release by using the same stimulation source but a distinct LC geometry. Local heating of a droplet-shaped water-in-LC compartment by NIR beam generated a temperature gradient that resulted in an internal flow leading to the shearing-based droplet release through the aqueous phase boundary. Flow-induced release is superior to those created by chemical or contact heating with instantaneous *in situ* adjustment of the release by tuning the laser intensity. Beyond dual-mode operation, contactless heating combined with beam spot size adjustability (1 - 9 mm) offered flexibility in using LC with various sizes and shapes (e.g., circular, rectangular, droplet), and enabled remotely controlled mixing of the reagents used for chemical assays, which we demonstrated in an exemplary assay.

2. Results and Discussion

Scheme 1 illustrates the pulsed release principle by using the contactless heating we employed in the study. Water droplets containing red dye and 9 mM sodium dodecyl sulfate (SDS) for homeotropic anchoring were initially emulsified in nematic LC phase (See the Experimental Section). Escape of the droplets to a neighboring aqueous phase is blocked by a mechanism that is associated with the elastic forces on the SDS-containing droplets applied by LC as described previously (Scheme 1a).^[44] When NIR light was illuminated on photothermal dye-LC hybrid from the air-LC interface, temperature reached above 32°C through photothermal heating and caused nematic-to-isotropic phase transition (Scheme 1b). Due to the thermal diffusion process, isotropic phase progressively expanded towards the aqueous interface (Scheme 1b). This I-N phase boundary can reduce the initial elastic forces on the droplets and drag droplets in the nematic phase.^[26] Accordingly, a certain portion of the droplets was released and merged with the aqueous solution while the rest remained suspended in the isotropic phase (Scheme 1c). After the laser was turned off, nematic phase was recovered back with the I-N phase boundary moving away from the LC-aqueous phase interface due to the lower surrounding temperature (Scheme 1d-e).



Scheme 1. Illustration of NIR-responsive pulsed-release of aqueous microdroplets from PDIB-hybridized nematic LC based on photothermal heating and LC phase change. Release stops after LC completely transits from the nematic phase to isotropic phase and after the laser is off, LC turns back to the nematic phase.

We synthesized the photothermal PDIB dye following the procedure described in the previous report^[45] characterized using FTIR and XPS as shown in Figure S1 and S2. PDIB formed a green solution when dissolved in organic liquids and exhibited a strong absorption peak around 940 nm (Figure 1a, inset shows a photograph of PDIB dissolved in toluene). NIR

light can penetrate in biological tissues within 1 cm-depth, and therefore is widely used in biomedical applications.^[46] The absorption spectrum of PDIB matches well with the wavelength of NIR light for such applications. In this study, a diode laser with 915 nm-wavelength was used to maintain both high absorbance and safer operating condition with lower photon energy compared to shorter wavelengths. Decomposition temperature of PDIB was measured to be 298°C using thermogravimetric analysis (Figure S3), enabling a wide thermal operating range. PDIB was physically hybridized with 5CB by mixing both in toluene and subsequently evaporating toluene under vacuum. Nematic-isotropic phase transition temperatures (T_{NI}) of PDIB-5CB hybrid mixtures were measured using a differential scanning calorimeter. T_{NI} of pure 5CB was 33.8°C, which gradually shifted from 33°C to 31°C by increasing PDIB concentration from 0.075% to 1.2% wt. (Figure 1b). The decrease of T_{NI} was attributed to the insignificant disruption of the LC phase with increasing dye which was similarly observed with the addition of halogen-bonded dye to 5CB.^[47]

Importantly, homogeneous green color of the PDIB-5CB hybrid confirmed the fine dispersion of PDIB (Figure 1c-i). The opaqueness of the mixture evident in Figure 1c-i arose from the nematic ordering of 5CB at room temperature. The hybrid mixture filling a reservoir of 5 mm-diameter and 5 mm-height was illuminated with a 3 mm-spot sized laser beam from the top. Appearance of the transparent green coloring at the top regions of the cylindrical compartment upon illumination as shown in Figure 1c-ii indicated that PDIB-5CB mixture was heated to its isotropic phase via photothermal process. Isotropic phase on the top was distinguishable from the bottom nematic phase by the spatial abrupt change in transparency observable with naked eyes. The line where transparent LC was separated from the opaque part was the so-called I-N phase boundary. I-N phase boundary moved vertically until 5CB was completely turned to isotropic with prolonged heating. I-N phase boundary shift velocity was determined using an image analysis software (ImageJ) after video recording under laser exposure. When laser power was increased from 94 mW to 184 mW for the 3 mm-spot sized NIR beam, velocity increased to 0.03 mm s⁻¹ from 0.02 mm s⁻¹ (Table S1). When the beam size was decreased from 3 mm to 2 mm for the power of 94 mW, velocity decreased from 0.02 mm s⁻¹ to 0.003 mm s⁻¹ which can be explained by the decreased spatial heating rate (Table S1).

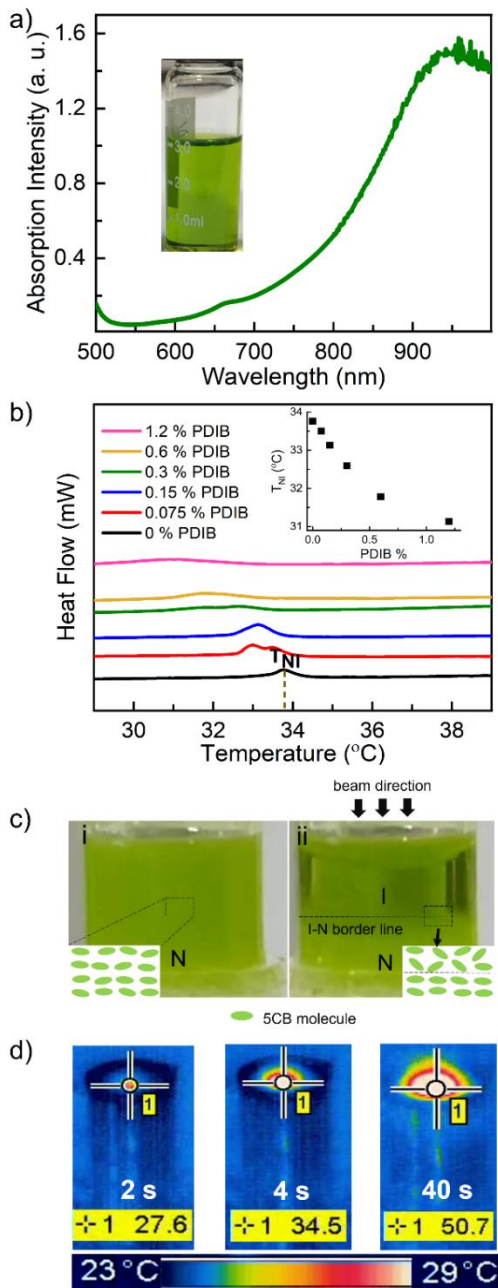


Figure 1. a) Absorption spectrum of PDIB solution. Inset shows a picture of PDIB solution in toluene. b) Differential scanning calorimetry thermographs of pure 5CB, and PDIB-5CB mixtures with 0.075%, 0.15%, 0.3%, 0.6%, and 1.2% wt. PDIB loading. Inset shows the change of nematic-isotropic phase transition temperature (T_{NI}) with increasing PDIB loading. c) (i) PDIB-5CB hybrid mixture in a plastic reservoir of 5 mm-diameter and 5 mm-height. Inset represents the nematic (N) ordering of the 5CB molecules at room temperature. (ii) The reservoir was illuminated with a 3 mm-spot sized laser beam from the top. Inset represents the ordering of the 5CB molecules in isotropic (I) phase and neighboring nematic phase in the dashed rectangle. d) Time-dependent images of PDIB-5CB mixtures recorded with a thermal

camera. Temperature values on the spots denoted by +1 sign on the thermal maps of the exposed area are indicated in the corresponding yellow boxes.

Another unique feature of the presented release system is the precise tunability of the heating rate. To investigate the heating rate with varying laser power intensity and PDIB loading, temperatures of PDIB-5CB mixtures were recorded using a thermal camera. Temperature distribution in the samples with the hottest spot denoted by the +1 sign on the thermal map was recorded as shown in representative images in Figure 1d. Temperature was measured on PDIB-5CB for 120 s under exposure to a 3 mm-spot sized laser beam at different laser intensities. Temperature reached the T_{NI} around 32 °C (for 0.15% wt. PDIB loading) in 55 s at a laser intensity of 1.8 W cm⁻² and same temperature in less than 5 s at 3.5 W cm⁻² (Figure 2a). Heating rate and maximum temperature increased with increasing laser intensity (Figure 2b and Figure S4) and with increasing PDIB loading (Figure 2c and Figure S4). When PDIB content was increased from 0.075% to 0.15% wt. under exposure to the 3 mm-spot sized beam with a power of 184 mW, I-N phase boundary shift velocity increased from 0.003 mm s⁻¹ to 0.01 mm s⁻¹ which was attributed to the higher light absorption (Table S1). As shown in Figure S5, the absorption intensity of the PDIB-5CB hybrid mixture at 915 nm increased with increasing PDIB concentration. PDIB-5CB showed reversible photothermal heating against repeated laser-on actions as demonstrated with five successive heating-cooling cycles where cooling took place passively at room conditions in the laser-off state (Figure 2d). No significant changes in the heating rate or maximum temperature were observed after the repeated measurements indicating the significant stability of the dye in 5CB, resulting in a non-hysteretic operation of the presented release system.

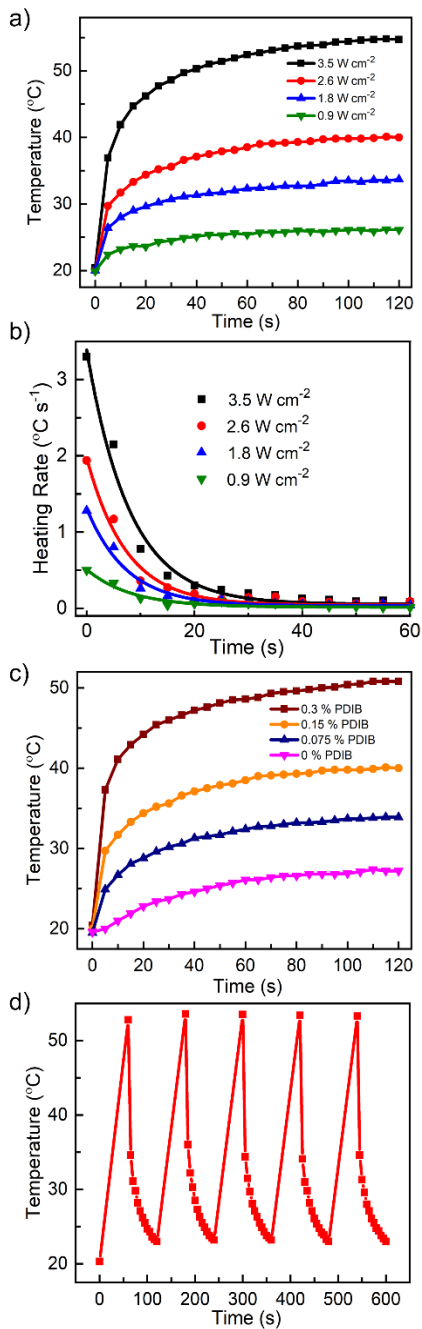


Figure 2. a) Temperature of PDIB-5CB (with 0.15% PDIB) measured every 5 s for 120 s under exposure to the 3 mm-spot sized laser beam at different laser power intensities. b) Exponential fitting of the heating rates depending on time for different power intensities. c) Temperature of PDIB-5CB and plain 5CB measured every 5 s for 120 s under exposure to the 3 mm-spot sized laser beam at an intensity of 2.6 W cm⁻² for different PDIB loading. d) Temperature of PDIB-5CB (with 0.15% PDIB) measured during five consecutive heating-cooling cycles by exposing to the laser beam at an intensity of 3.5 W cm⁻². Temperature values were recorded at a room condition with a temperature of 19 °C.

Based on the propagation of the isotropic phase throughout the LC, a NIR-responsive microdroplet release system was designed. The system is a water-in-LC emulsion prepared by loading red-dyed water droplets in PDIB-5CB mixture. Figure 3a shows the photothermal LC emulsion placed at the bottom of a glass tube filled with water and turned upside down. The emulsion was excited with the laser beam from the glass side. The generated I-N phase boundary was propagated towards the aqueous phase and clearly showed the suspended, red microdroplets in PDIB-hybridized green 5CB. Because of the I-N phase boundary shift, the dyed droplets were released into the water underneath. 5CB remained structurally intact during the release, unlike many other gatekeeper materials which undergo structural disruption to release the agents under stimuli.^[9-14] A consecutive release pulse was also achieved by turning off the NIR light to allow the LC to transit back to the nematic phase and then turning on the laser again (Supporting Video 1).

To investigate the characteristics of the NIR-induced, pulsed release in more detail, we casted water(dyed)-in-PDIB/5CB emulsions on aqueous solutions in cuvettes of 4 mL-volume through mini-wells and left their top open to air. For this, the emulsions were filled in square or circular shaped gaps of various surface areas formed in PDMS molds (Figure 3b). The emulsions were excited from their top with a 9 mm-spot sized laser beam at an intensity of 0.7 W cm^{-2} . Release performance of the hybrid emulsions was investigated by measuring the released mass of red ponceau dye with spectrophotometry after seven laser on/off cycles. Beam spot size was kept larger than the surface area occupied by LC for homogenous exposure. Released mass decreased with sequential pulses due to the gradual reduction of the total droplet number (Figure 3c). Released mass in each pulse increased linearly with the LC area (Figure 3d). The lower release rate with smaller area was also obvious upon visual monitoring (Figure 3b). Interestingly, we observed release to occur near the edges of the LC. Cross-sectional imaging of LC revealed a meniscus where LC was thicker near the PDMS walls (Figure 3e). Accordingly, droplets near the walls were exposed to the elastic pressure by the moving dome-shaped I-N phase boundary and therefore passed to the aqueous phase earlier than those in the center due to a droplet congestion formed behind them (Figure 3e). Then, droplets in the center followed a path along the LC-aqueous phase interface towards the walls and were released from the edge. We also found the released mass in each pulse to increase linearly with the LC thickness at constant area (Figure 3f) since higher droplet congestion occurred by the moving I-N border due to the droplet collection from a larger volume. Release starting time after laser was turned on, depended on the laser power and the LC thickness while the LC area had a negligible effect. For instance, release was observed after 71 s and 76 s in 1 mm-thick 0.07 cm^2

LC and 0.19 cm^2 LC, respectively at 0.7 W cm^{-2} laser intensity. Release was observed after 118 s when the thickness of the LC was increased to 3 mm and after 30 s when the excitation intensity was increased to 1.4 W cm^{-2} at constant thickness. Thus, an increase in the light intensity consistently led to an increase in the heating rate and -N phase boundary shift velocity while the increase in thickness extended the path through which I-N boundary moved. It is noteworthy that release dosage was controlled from $0.5 \mu\text{g}$ per pulse to $2.5 \mu\text{g}$ per pulse and the total dosing was dependent on the number of the pulses.

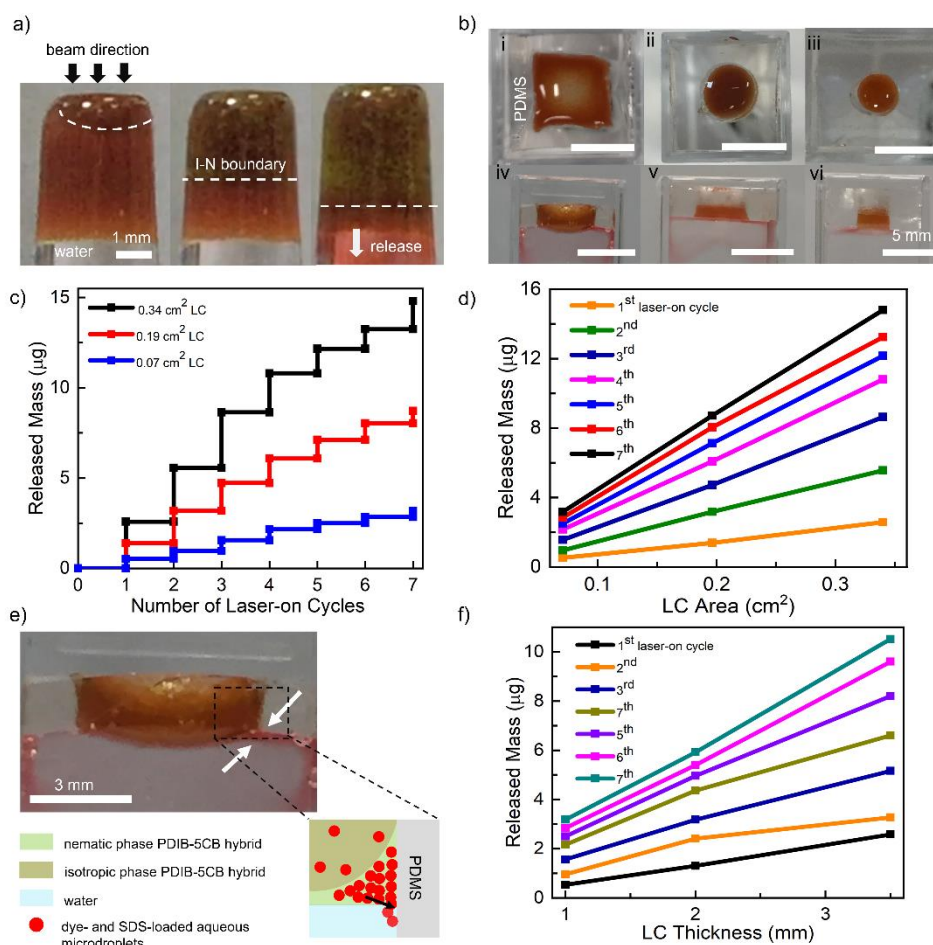


Figure 3. a) Water-in-LC emulsion prepared by loading red-dyed water droplets in PDIB-5CB hybrid. The emulsion was sequestered between the bottom of a glass tube and water and excited with a 3 mm-spot sized laser beam from the glass side. White dashed line shows the isotropic-nematic (I-N) border moving towards the aqueous phase underneath and allowing the red droplets to merge with the aqueous phase. b) (i-iii) Top-view and (iv-vi) side-view of water-in-LC emulsions casted on mini-wells with area of 0.34 cm^2 , 0.19 cm^2 and 0.07 cm^2 , respectively. c) Release profiles depending on the number of laser on-off cycles for different LC area. d) Dependence of the released mass on the LC area for seven laser-on cycles. e) Side-view of water-in-LC emulsion during release. The dense red color on the edge between the white arrows shows the released dye. Scheme represents the droplet profile at the PDMS-LC-aqueous phase

interface. f) Dependence of the released mass on the LC thickness for seven laser-on cycles. Emulsions were under illumination with a 9 mm-spot sized beam at an intensity of 0.7 W cm^{-2} . Released mass values represent red dye amount in micrograms (μg) in 4 mL of water.

Adjustment of the beam spot size on a relatively larger LC area resulted in the spatial control of the I-N phase boundary shifting and pulsated release. As shown in Figure 4a (ii-iv, left images), evident green color of the area exposed to a 7 mm-spot-sized NIR beam indicated a reduced droplet population in the isotropic phase due to the sweeping towards the outer regions by the moving I-N phase boundary. A schematic of the I-N phase border movement and droplet distribution is shown in Figure 4a (ii-iv, right sketches). Droplet congestion was observed to occur in a ring pattern surrounding the green circle when the LC was observed from the top as shown in Figure 4a-iii. Droplet congestion was increased by further propagation of the I-N phase boundary as evident from the darker red appearance around the green ring. The expansion of the isotropic phase increased the elastic pressure on the droplets adjacent to the aqueous border, therefore, led to their escape to the aqueous phase in a ring pattern (Figure 4a-iv). Such release of the dye was evident as a dense red ring with a diameter of ~ 7 mm when observed from the top as denoted with the white arrows in Figure 4a-iv. Difference between the size of release rings upon illumination with an either 7 mm- or 3 mm-spot sized beam was also distinguishable when the emulsions were imaged from their bottom side as shown in Figure 4b (i-ii). A release ring of ~ 3 mm- diameter under exposure to a 3 mm-spot sized beam was also viewed from the top as denoted with the white arrows in the middle of the green area shown in Figure 4b-iii. Consequently, site of the droplet gathering, and release were spatially controlled by the beam spot size when the spot area was smaller than the LC area. Green color of the nematic phase surrounding the release ring was more evident over time due to droplet collection at the outer regions of the isotropic phase by the expanding I-N phase boundary (Figure 4b-iii). Through these experiments we found the released mass per pulse to increase linearly with the beam spot area ranging from 0.07 cm^2 for 3 mm-spot size to 0.38 cm^2 for 7 mm-spot size (Figure 4c).

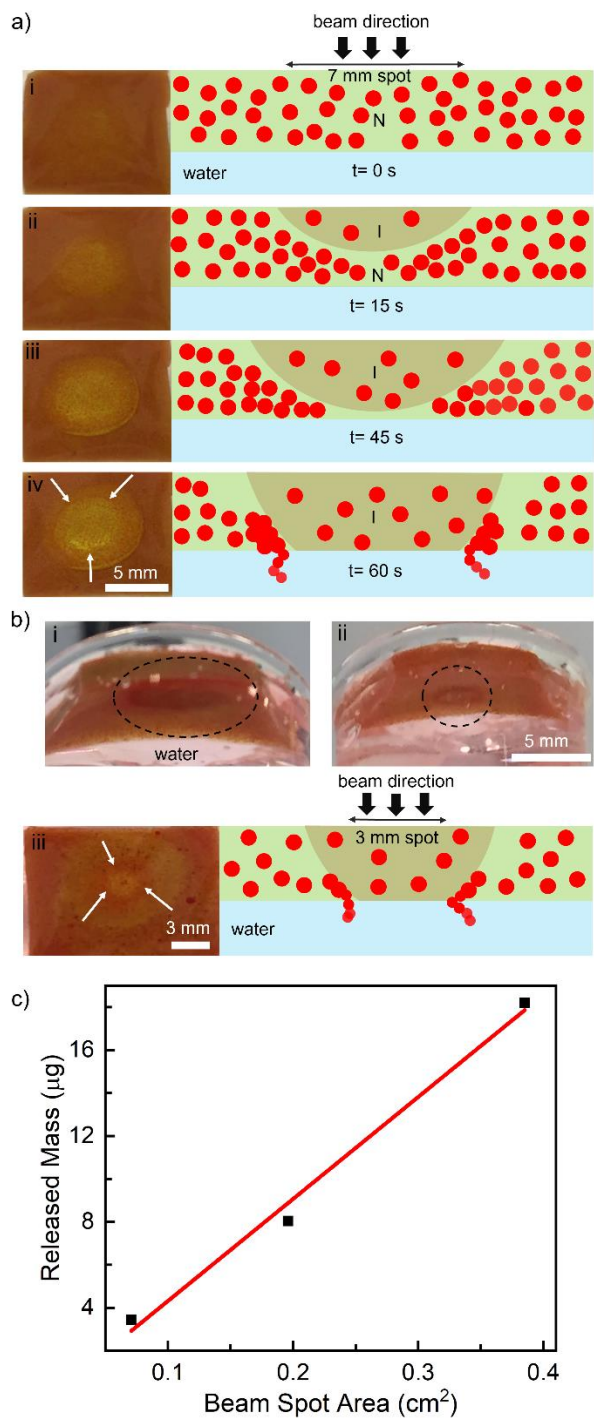


Figure 4. a) (i-iv, left) Top-view of large-area water-in-LC emulsion under time-dependent heating by the excitation with a 7 mm-spot sized laser beam. White arrows denote the red release ring formed at the I-N-aqueous phase interface. (i-iv, right) Corresponding schematic representation of the droplet (denoted as red spheres) profile at the LC cross-section. I and N represent the isotropic and nematic phases, respectively. b) View of the water-in-LC emulsions from their bottom surface showing the release rings in black dashed circles by the excitation with a (i) 7 mm-spot sized or (ii) 3 mm-spot sized beam. (iii) Top-view and corresponding cross-sectional representation of the water-in-LC emulsion by the excitation with a 3 mm-spot

sized laser beam. White arrows denote the red release ring formed at the I-N-aqueous phase interface. c) Linear fitting of released mass as a function of beam spot area. Release mass was measured after seven release pulses for each beam spot area. Mass values represent red dye amount in micrograms (μg) in 4 mL of water.

We demonstrated the versatility of the microdroplet release system for on-demand mixing of the reagents to obtain their *in-situ* generated reaction signal. *In-situ* polymerization of dopamine (DA) was shown for the quantitative hydrogen peroxide (H_2O_2) assay. H_2O_2 is an extensively used chemical and produced in various enzymatic processes (e.g., glucose oxidation).^[48-50] DA is rapidly oxidized to quinone at basic pH and produces polydopamine (PDA) by undergoing several chemical and physical bonding interactions.^[51,52] In the presence of H_2O_2 , *in-situ* generated PDA fluorescence increases due to scavenging reactions between peroxy-radicals and PDA.^[53] We prepared an array of mini-wells of 5 mm- diameter and 4 mm-height and placed it above the H_2O_2 solution. Mini-wells were loaded with two separate water-in-LC emulsions loaded with DA and Tris-HCl (pH 8.6) buffer droplets (Figure 5a, inset). Buffer and DA droplets were released and mixed with the H_2O_2 solution in sequence (Figure 5a and Figure 5b). Aqueous phase maintained a pink hue after the release due to the presence of the tracer red dye within the droplets and then turned to brown after PDA generation (Figure 5c). The fluorescence of PDA was centered around 490 nm and its intensity was found to increase with increasing H_2O_2 concentration from 1 mM to 5 mM (Figure 5d). We note here that a prolonged PDA incubation upon premixing of DA with buffer quenches the fluorescence causing loss of sensitivity against H_2O_2 (Figure 5d). Therefore, it was critical to store DA and buffer in isolated wells and mix on-demand, which we showed herein as a successful application using the water-in-LC emulsion release system. Notably, laser-based heating adds value to the serially managed processes and holds significant advantage over chemical stimuli which trigger the release by diffusing to the sites unselectively.

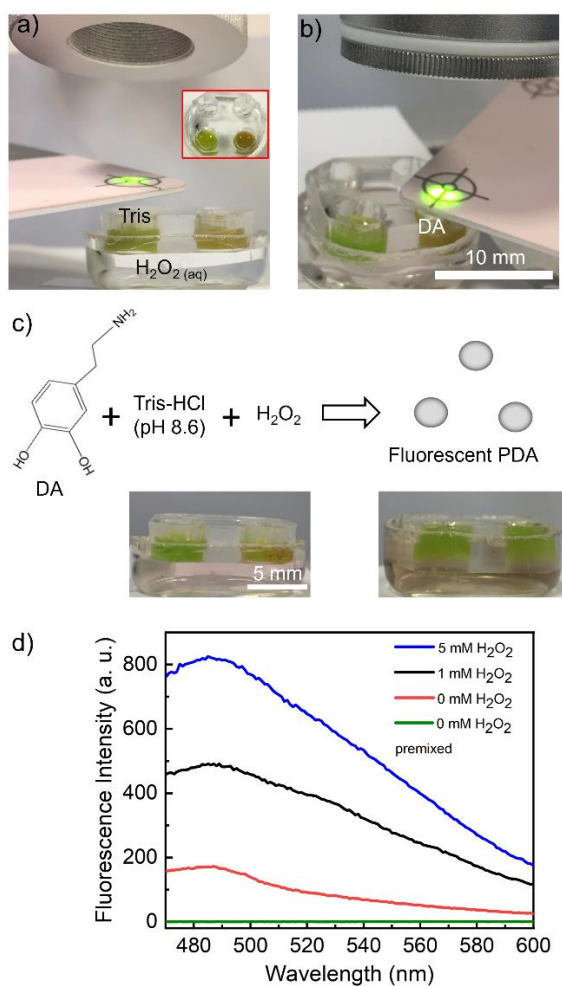


Figure 5. a) Water-in-LC emulsion loaded with Tris-HCl buffer droplets on the left mini-well excited with NIR laser. Green spot indicates the NIR laser beam. Inset: Top-view of the mini-wells filled with the emulsions loaded with Tris-HCl buffer and DA droplets. b) Water-in-LC emulsion loaded with DA droplets on the right mini-well excited with NIR laser. c) Oxidation reaction of DA in Tris-HCl buffer in the presence of H₂O₂. Pictures show the aqueous solutions during the release of DA and Tris buffer and after PDA formation. d) Fluorescence spectra of the *in-situ* formed PDA in the absence and presence of H₂O₂ with concentration of 1 mM and 5 mM and fluorescence of PDA measured after premixing and incubation of DA and Tris-HCl buffer.

Microcapsules, particles, and droplets have been the workhorses of photothermal therapy, drug release, and bioimaging since their size and shape fulfill the circulation, delivery, and uptake criteria in biological paths. Thus, in the last part of this study, we investigated the potential of the water-in-LC-in-water double emulsions in on-demand release. We prepared the double emulsions by dispersing the pre-prepared water(dyed)-in-LC emulsion in aqueous phase. The diameters of the water-in-LC droplets were kept around 1-3 mm to monitor the release

characteristics visually under local heating. Droplets positioned at the bottom of the aqueous solution and observed to yield a hemispherical shape (Figure 6a). Dye-loaded water microdroplets in LC were mostly packed on the top regions of the LC droplets due to the buoyancy effects. When the droplet-shaped LC was illuminated with a 1 mm-spot sized beam on its side (heated from the right edge in Figure 6b), water droplets within the LC were ejected from the top after gradually increasing the beam intensity from $\sim 23 \text{ W cm}^{-2}$ to 70 W cm^{-2} , which was attributed to the largest droplet crowd on the top (Figure 6e-f and Figure S6). Surprisingly, ejection of the water droplets continued during the illumination with NIR beam revealing a continuous release mode that is distinct from the pulsated-mode described above for the release medium filled in mini-wells and illuminated from the top side.

While the laser was illuminated on the right side of the droplet as shown in Figure 6b, water droplets in the LC medium were observed to flow counterclockwise (Supporting Video 2). The internal flow was ascribed to the convective heat transfer generated by the temperature gradient within the LC medium (Figure 6f). The magnitude of the temperature gradient was important in continuous-mode release as we observed a slowing down of the flow that led to the release termination when illumination intensity was reduced to around 40 W cm^{-2} as shown in Figure 6c-d. We observed the release initiation after increasing the intensity back to 70 W cm^{-2} (Supporting Video 2). As a control experiment, we illuminated the LC droplet with a 3 mm-spot sized beam and observed an absence of release at $\sim 8 \text{ W cm}^{-2}$, corresponding to the current (1030 mA) close to that where we started to observe release upon exposure to 1 mm-spot sized beam (Figure S6). Because the internal flow was observed to be weaker due to the lower laser intensity compared to that generated under illumination by a 1 mm-spot sized beam (Supporting Video 3). These observations revealed that a stronger internal flow formed in the LC droplet, induces a shear to the aqueous phase boundary leading to microdroplet release through shearing-induced breakage of the elastic LC strains. Such observations were consistent with the past report showing the droplet release due to the external shear applied by the bacterial motion at the LC-aqueous phase interfaces^[26], highlighting the shear-induced release mechanism with the internally-generated flow we observed in our system.

Importantly, light intensities above 100 W cm^{-2} using a 1 mm-spot sized beam in motivation to enhance the release rates with stronger flow resulted in the induction of a bulk flow of the isotropic and nematic phases as shown in Figure 6g-h (additional visuals are available in Supporting Video 2 and Figure S6). Such flow appeared to hinder the transport of the LC-dispersed water microdroplets towards the LC-aqueous phase interface and resulted in the release termination despite of the strong flow. Such observations revealed the importance

of an intermediate laser intensity range that permits both the droplet migration towards the LC-aqueous phase interface and generation of the shear force to break the elastic LC strains at the interfaces. It is noteworthy to highlight that such a convection-based release from droplet-shaped LC can only be achieved with localized stimulation by remote source (e.g., light). Continuous release presents a unique mechanism in the sense of instantaneous excitation adjustment and excellent *in situ* on/off control in a single shot with no wait time as in the diffusion-mediated or phase change processes. Thus, continuous-mode renders the LC-based release system versatile with a high spatiotemporal sensitivity developed using a single type of stimulation source.

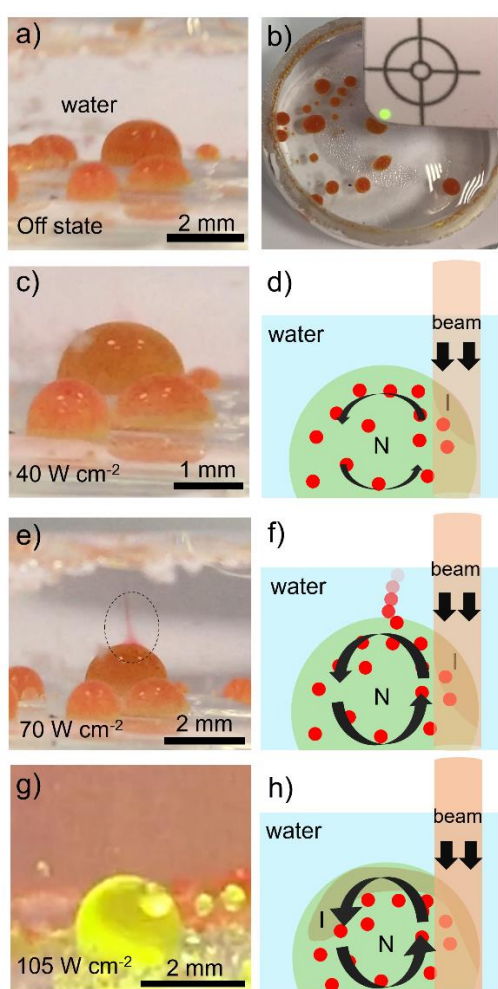


Figure 6. a) Droplet-shaped water (dyed)-in-LC immersed in aqueous solution at laser-off state. b) Illumination of LC droplet locally at its right edge with a 1 mm-spot sized beam. Green spot indicates the NIR laser beam. c) Photograph of a LC droplet upon exposure to laser beam at an intensity of 40 W cm^{-2} showing no release. d) Schematic representation of the low-speed internal flow because of the relatively low laser intensity. e) Photograph of a LC droplet upon exposure to laser beam at an intensity of 70 W cm^{-2} showing the continuous-mode release of

the dyed aqueous droplets. f) Schematic representation of microdroplet release induced by internal flow. g) Photograph of a LC droplet upon exposure to laser beam at an intensity of 100 W cm^{-2} showing the cessation of the release due to bulk I-N flow. h) Schematic representation of the internal structure of the LC droplet during the bulk flow. I and N represent the isotropic and nematic phases, respectively.

3. Conclusion

We developed a stimuli-responsive droplet release mechanism using thermotropic liquid crystals. A lyophilic photothermal dye that was physically hybridized with liquid crystal produced heat by NIR laser excitation, and the heating rate was tuned by adjusting the laser intensity and dye concentration. Photothermally-generated heat was exploited to deform elastic strains in liquid crystal and allow the initially entrapped aqueous microdroplets to merge with the bulk aqueous phase. Droplet release was modulated in two distinct ways (pulsated- and continuous) with high spatiotemporal resolution by liquid crystal geometry design, heating localization, and heating rate control. Released dosage was precisely regulated by tuning the liquid crystal dimensions, laser beam spot size and laser on/off cycles. Dye-liquid crystal hybrid showed robust thermal stability under repeated heating cycles and multiple-time use. For continuous-mode release, we found an intermediate laser intensity regime critical to transport the microdroplets to the liquid crystal-aqueous interface and to generate shear for their release. Contactless, NIR-mediated stimulation we report here enabled a significantly rapid adjustment of the release by laser intensity and has the potential to lead to a breakthrough in the advancement of the liquid crystal-based materials for critical applications in drug release, controlled mixing, micro-scale controlled synthesis and photothermal therapy among the others.

4. Experimental Section

Synthesis of PDIB Dye: PDIB was produced via the oxidation and ion exchange reactions of neutral amine (IPA) according to the previously reported method.^[45] N,N,N',N'-tetrakis(p-diisobutylaminophenyl)-p-phenylenediamine (1 g) was first added to a 3-neck glass flask. Then, lithium bis(oxalate)borate (500 mg), dichloromethane (3.5 mL) and ethanol (2.5 mL) were added, and the mixture was refluxed for 2 h. Afterwards, sodium persulfate (330 mg) and deionized (DI) water (6.7 mL) were added, and the mixture was refluxed for further 2 h. The reaction was terminated by adding dichloromethane (150 mL) and DI water (200 mL). The mixture was vigorously shaken to transfer the unreacted species to water. The organic phase in the mixture was separated from the aqueous phase by using a separatory funnel. Dichloromethane in the organic phase was completely evaporated by using a rotary evaporator. PDIB dye was obtained as a dark green powder.

Preparation of Photothermal PDIB-5CB Hybrids: PDIB (20 mg) was dissolved in toluene (1 mL). Different portions of PDIB solution were mixed with 5CB (100 μ L) to have liquid crystals with final PDIB concentration of 0.075%, 0.15%, 0.3%, 0.6%, and 1.2% wt. The mixtures were ultrasonicated for 10 min to dissolve 5CB completely in toluene and then toluene was evaporated in vacuum oven overnight.

Photothermal Measurements: Fiber-coupled diode laser (CNI lasers, MDL-III-915-1W) was used for all photothermal excitations at 915 nm and a thermal camera (FLIR Systems, Thermovision A40) was used to record the temperature of the PDIB-5CB hybrid mixtures. Glass mini-wells were filled with PDIB-5CB (20 μ L) and placed under laser aperture at a 10 cm-distance. Laser beam spot size was adjusted to 3 mm. After the laser was turned on, temperature was recorded for 120 s. Laser power was adjusted to 62 mW, 124 mW, 186 mW, and 248 mW for the measurement at different power intensities. For the measurements for different dye concentration, power and beam spot size were adjusted to 186 mW and 3 mm, respectively and LCs with 0.075%, 0.15%, and 0.3% wt. PDIB were measured. LC without PDIB was also measured as a control sample.

Preparation of PDMS Molds: Sylgard elastomer base (10 g) was mixed with curing agent (1 g) and degassed in a vacuum oven followed by casting on a glass petri dish. The mixture was cured at 100 °C for 10 min. Two 1x1 cm PDMS pieces were cut, and circular holes of 5 mm- and 3 mm-diameter were punched at their centers using biopsy punches. A 6x6.5 mm square hole was created on a different 1x1 cm PDMS piece using a razor blade.

Release Experiments: For release experiments, 5CB including 0.15% wt. PDIB was used. First, red ponceau dye (20 mg) was dissolved in SDS solution (0.5 mL, 9 mM). 2.5 μ L of that was

added to PDIB-5CB (47.5 μL) and vortexed at 3000 rpm for 1 min to obtain water-in-PDIB/5CB emulsion with 5% vol. water droplet. Prepared PDMS mini-wells were placed on the opening of spectrophotometry cuvettes (4 mL-volume) filled with water. Water-in-PDIB/5CB emulsions were drop-casted on water through the holes in a final thickness of 1 mm. Cuvettes were placed under laser aperture at a 10 cm-distance. Beam spot size was adjusted to 9 mm and laser power was set as 460 mW. Release of the red dye to water was monitored visually after the laser was turned on. After the release was completed, laser was turned off. Absorbance of the released dye at 506 nm was measured. Laser on/off cycles were repeated seven times and absorbance was measured after every release pulse. Released mass was determined using the calibration curve generated by the absorbances of red ponceau solutions with known concentration. For the release measurements for different LC thicknesses, mini-wells of 3 mm-diameter were filled with 10 μL , 20 μL , and 30 μL of the emulsions to have thicknesses of 1 mm, 2 mm, and 3 mm, respectively. A PDMS mold with 1.2x1.2 cm square hole was placed on the opening of a 5 mL-beaker filled with water and 200 μL of the emulsion was drop-casted on water through the hole. The LC emulsion was first excited with 3 mm-spot sized beam with a power of 69 mW to have an intensity of 0.9 W cm^{-2} and the released mass was measured after seven on/off cycles. Experiments were repeated with 5 mm- and 7 mm-spot sized laser beam with a power of 143 mW, and 287 mW, respectively to obtain power intensity of 0.7 W cm^{-2} .

Preparation of Droplet-Shaped LC: Water-in-PDIB/5CB emulsion was vortexed in water at 1000 rpm for 5 s to form water-in-LC-in-water double emulsion and poured into a glass reservoir filled with water.

Hydrogen Peroxide (H_2O_2) Assay: Mini-wells were prepared by punching holes of 5 mm-diameter and 4 mm-height on a PDMS piece. PDMS was placed on the top of a glass dish filled with H_2O_2 solution (1 mM). SDS (9 mM) was prepared in Tris-HCl buffer (0.5 mL, 500 mM, pH 8.6) and red ponceau (5 mg) was added. 10 μL of that solution was vortexed in PDIB-5CB (90 μL) to have a droplet concentration of 10% vol. and finally the emulsion was drop-casted in one mini-well. SDS (9 mM) was prepared in DA solution (0.5 mL, 100 mM) and red ponceau (5 mg) was added. 10 μL of that solution was vortexed in PDIB-5CB (90 μL) and the emulsion was drop-casted in a second mini-well. First, the Tris-HCl mini-well was excited with a 6 mm-spot sized laser beam with a power of 69 mW. Then, the power was gradually increased to 282 mW to ensure that the LC phase turned to isotropic at the LC-aqueous interface. Droplet release was monitored with the help of the red tracer dye. Droplets were completely released after five successive heating and cooling steps. After buffer release, DA droplets were released similarly.

After 3 h-incubation at room temperature, fluorescence of the produced polydopamine was measured. Experiments were repeated in the absence and presence of H₂O₂ with a concentration of 5 mM.

Characterization: Fluorescence measurements were done using a fluorescence spectrophotometer (Varian Eclipse). Polydopamine solutions were excited at 420 nm. Absorption signals of the PDIB dye, released red ponceau dye and PDIB-5CB films were recorded using an UV-Vis-NIR absorption spectrophotometer (Varian Eclipse, Cary5000). PDIB-5CB films were prepared as a sandwiched structure between two glass slides by capillary suction. Thermographs of the PDIB-5CB hybrid mixtures were recorded using a differential scanning calorimeter (Perkin Elmer, DSC8000) with a scan rate of 5 °C min⁻¹ at nitrogen atmosphere. Decomposition temperature of PDIB was measured using a thermogravimetric analyzer (TA Instruments, Q500) with a scan rate of 10 °C min⁻¹ at nitrogen atmosphere.

Supporting Information

Supporting Information is available from the Wiley Online Library or from the author.

Acknowledgements

This work was supported by the Scientific and Technological Research Council of Turkey (TÜBİTAK) BİDEB-National Postdoctoral Research Program under the Project No.118C462.

Received: ((will be filled in by the editorial staff))

Revised: ((will be filled in by the editorial staff))

Published online: ((will be filled in by the editorial staff))

References

- [1] J. Liu, C. Detrembleur, S. Mornet, C. Jerome, E. Duguet, *J. Mater. Chem. B* **2015**, 3, 6117.
- [2] Z. Li, E. Ye, David, R. Lakshminarayanan, X. J. Loh, *Small* **2016**, 35, 4782.
- [3] S. Senapati, A. K. Mahanta, S. Kumar, P. Maiti, *Signal Transduction Targeted Ther.* **2018**, 3, 7.
- [4] A. Raza, U. Hayat, T. Rasheed, M. Bilal, H. M. Iqbal, *J. Mater. Res. Technol.* **2019**, 8, 1497.
- [5] X. Fu, L. Hosta-Rigau, R. Chandrawati, J. Cui, *Chem* **2018**, 4, 2084.
- [6] X. Li, C. Xie, H. Xia, Z. Wang, *Langmuir* **2018**, 34, 9974.

- [7] M. Qiu, D. Wang, W. Liang, L. Liu, Y. Zhang, X. Chen, D. K. Sang, C. Xing, Z. Li, B. Dong, F. Xing, D. Fan, S. Bao, H. Zhang, Y. Cao, *Proc. Natl. Acad. Sci. USA* **2018**, *115*, 501.
- [8] S. Geng, H. Zhao, G. Zhan, Y. Zhao, X. Yang, *ACS Appl. Mater. Interfaces* **2020**, *12*, 7995.
- [9] M.-C. Chen, H.-A. Chan, M.-H. Ling, L.-C. Su, *J. Mater. Chem. B* **2017**, *5*, 496.
- [10] M.-C. Chen, Z.-W. Lin, M.-H. Ling, *ACS Nano* **2016**, *10*, 93.
- [11] Y. Dai, J. Su, K. Wu, W. Ma, B. Wang, M. Li, P. Sun, Q. Shen, Q. Wang, Q. Fan, *ACS Appl. Mater. Interfaces* **2019**, *11*, 10540.
- [12] Q. Wang, Y. Dai, J. Xu, J. Cai, X. Niu, L. Zhang, R. F. Chen, Q. M. Shen, W. Huang, Q. Fan, *Adv. Funct. Mater.* **2019**, *29*, 1901480.
- [13] Y. Zhang, G. Jiang, W. Hong, M. Gao, B. Xu, J. Zhu, G. Song, T. Liu, *ACS Appl. Bio Mater.* **2018**, *1*, 1906.
- [14] J. Liu, C. Detrembleur, M.-C. De Pauw-Gillet, S. Mornet, L. V. Elst, S. Laurent, C. Jérôme, E. Duguet, *J. Mater. Chem. B* **2014**, *2*, 59.
- [15] J. Ping, L. Qi, Q. Wang, S. Liu, Y. Jiang, L. Yu, J.-M. Lin, Q. Hu, *Biosens. Bioelectron.* **2021**, *187*, 113313.
- [16] M. Tsuei, H. Sun, Y.-K. Kim, X. Wang, N. C. Gianneschi, N. L. Abbott, *Langmuir* **2022**, *38*, 332.
- [17] W. Wu, W. Wang, L. Qi, Q. Wang, L. Yu, J. M. Lin, Q. Hu, *Anal. Chem.*, **2021**, *93*, 6151.
- [18] P. Bao, D. A. Paterson, P. L. Harrison, K. Miller, S. Peyman, J. C. Jones, J. Sandoe, S. D. Evans, R. J. Bushby, H. F. Gleeson, *Lab Chip* **2019**, *19*, 1082.
- [19] X. Wang, H. Sun, Y.-K. Kim, D. B. Wright, M. Tsuei, N. C. Gianneschi, N. L. Abbott, *Adv. Mater.* **2022**, *34*, 2106535.
- [20] O. M. Wani, R. Verpaalen, H. Zeng, A. Priimagi, A. P. H. J. Schenning, *Adv. Mater.* **2019**, *31*, 1805985.
- [21] Y. Wu, Y. Yang, Q. Chen, X. Qian, Y. Wei, Y. Ji, *Angew. Chem., Int. Ed.* **2020**, *59*, 4778.
- [22] L. L. Dong, Y. Zhao, *Mater. Chem. Front.* **2018**, *2*, 1932.
- [23] U. Manna, D. M. Lynn, *Adv. Mater.* **2015**, *27*, 3007.
- [24] F. Lancia, A. Ryabchun, N. Katsonis, *Nat. Rev. Chem.* **2019**, *3*, 536.
- [25] C. Esteves, E. Ramou, A. R. P. Porteira, A. J. Moura Barbosa, A. C. A. Roque, *Adv. Opt. Mater.* **2020**, *8*, 1902117.
- [26] Y.-K. Kim, X. Wang, P. Mondkar, E. Bokusoglu, N. L. Abbott, *Nature* **2018**, *557*, 539.
- [27] D. Franklin, T. Ueltschi, A. Carlini, S. Yao, J. Reeder, B. Richards, R. P. Van Duyne, J. A. Rogers, *ACS Nano* **2021**, *15*, 2327.

- [28] D. Zhao, F. Fan, J. Cheng, Y. Zhang, K. S. Wong, V.G. Chigrinov, H. S. Kwok, L. Guo, B. Z. Tang, *Adv. Opt. Mater.* **2015**, *3*, 199.
- [29] A. Hou, H. Chen, C. Zheng, K. Xie, A. Gao, *ACS Nano* **2020**, *6*, 7380.
- [30] Y. Xu, A. M. Rather, Y. Yao, J. C. Fang, R. S. Mamtani, R. K. A. Bennett, R. G. Atta, S. Adera, U. Tkalec, X. Wang, *Sci. Adv.* **2021**, *7*, eabi7607.
- [31] A. H. Gelebart, D. Q. Liu, D. J. Mulder, K. H. J. Leunissen, J. van Gerven, A. P. H. J. Schenning, D. J. Broer, *Adv. Funct. Mater.* **2018**, *28*, 1705942.
- [32] Y. Zhan, G. Zhou, B. A. G. Lamers, F. L. L. Visschers, M. M. R. M. Hendrix, D. J. Broer, D. Liu, *Matter* **2020**, *3*, 782.
- [33] L. Pezzi, L. De Sio, A. Veltri, T. Placido, G. Palermo, R. Comparelli, M. L. Curri, A. Agostiano, N. Tabiryan, C. Umeton, *Phys. Chem. Chem. Phys.* **2015**, *17*, 20281.
- [34] L. De Sio, P. F. Lloyd, N. V. Tabiryan, T. Placido, R. Comparelli, M. L. Curri, T. J. Bunning, *ACS Appl. Nano Mater.* **2019**, *2*, 3315.
- [35] N. Podoliak, O. Buchnev, O. Buluy, G. D'Alessandro, M. Kaczmarek, Y. Reznikov, T. Sluckin, *Soft Matter* **2011**, *7*, 4742.
- [36] Y. Ji, F. Fan, S. Xu, J. Yu, S. Chang, *Nanoscale* **2019**, *11*, 4933.
- [37] Y. Tao, H. F. Chan, B. Y. Shi, M. Q. Li, K. W. Leong, *Adv. Funct. Mater.* **2020**, *30*, 2005029.
- [38] H. T. Sun, M. X. Feng, S. Y. Chen, R. Z. Wang, Y. Luo, B. Yin, J. C. Li, X. L. Wang, *J. Mater. Chem. B* **2020**, *8*, 7149.
- [39] W. J. Jiang, F. Mo, X. Jin, L. Chen, L. J. Xu, L. Q. Guo, F. F. Fu, *Adv. Mater. Interfaces* **2017**, *4*, 1700425.
- [40] A. Wang, Q. Mao, M. Zhao, S. Ye, J. Fang, C. Cui, Y. Zhao, Y. Zhang, Y. Zhang, F. Zhou, H. Shi, *Anal. Chem.* **2020**, *92*, 16113.
- [41] H. Zeng, P. Wasylczyk, D. S. Wiersma, A. Priimagi, *Adv. Mater.* **2017**, *30*, 1703554.
- [42] J. Li, R. Zhang, L. Mou, M. Jung de Andrade, X. Hu, K. Yu, J. Sun, T. Jia, Y. Dou, H. Chen, S. Fang, D. Qian, Z. Liu, *Adv. Funct. Mater.* **2019**, *29*, 1808995.
- [43] B. Zuo, M. Wang, B. P. Lin, H. Yang, *Nat. Commun.* **2019**, *10*, 4539.
- [44] S. B. Chernyshuk, B. I. Lev, *Phys. Rev. E* **2011**, *84*, 011707.
- [45] M. Han, B. Kim, H. Lim, H. Jang, E. Kim, *Adv. Mater.* **2020**, *32*, 1905096.
- [46] A. Y. Rwei, W. Wang, D. S. Kohane, *Nano Today* **2015**, *10*, 451.
- [47] J. Vapaavuori, A. Siiskonen, V. Dichiarante, A. Forni, M. Saccone, T. Pilati, C. Pellerin, A. Shishido, P. Metrangolo, A. Priimagi, *RSC Adv.* **2017**, *7*, 40237.

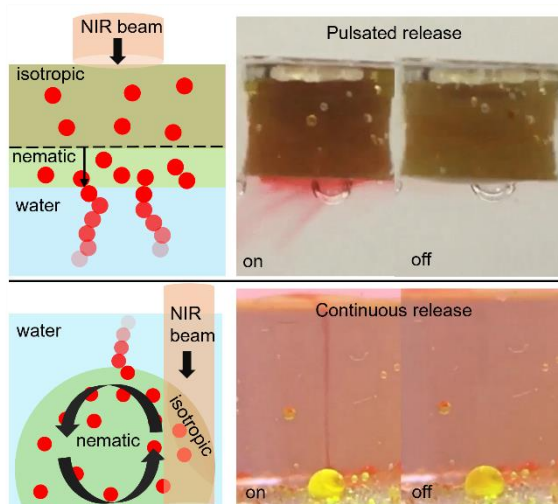
- [48] J. W. Liu, Y. Luo, Y. M. Wang, L. Y. Duan, J. H. Jiang, R. Q. Yu, *ACS Appl. Mater. Interfaces* **2016**, *8*, 33439.
- [49] Z. Song, R. T. Kwok, D. Ding, H. Nie, J. W. Lam, B. Liu, B. Z. Tang, *Chem. Commun.* **2016**, *52*, 10076.
- [50] J. Chang, H. Li, T. Hou, W. Duan, F. Li, *Biosens. Bioelectron.* **2018**, *104*, 152.
- [51] T. G. Barclay, H. M. Hegab, S. R. Clarke, M. Ginic-Markovic, *Adv. Mater. Interfaces* **2017**, *4*, 1601192.
- [52] S. Hong, Y. S. Na, S. Choi, I. T. Song, W. Y. Kim, H. Lee, *Adv. Funct. Mater.* **2012**, *22*, 4711.
- [53] J.-H. Lin, C.-J. Yu, Y.-C. Yang, W.-L. Tseng, *Phys. Chem. Chem. Phys.* **2015**, *17*, 15124.

A novel remotely controlled droplet release mechanism is presented. Photothermally-functionalized liquid crystal that generates heat under NIR laser excitation, is used for the on-demand release of water droplets via pulsated mode or continuous mode. The former is based on the transition of liquid crystal to isotropic phase while the latter is based on convection-induced shearing.

P. Beyazkılıç, S. Akcimen, C. Elbuken, B. Ortaç, S. Cai, E. Büküşoğlu*

Contactless Pulsed and Continuous Microdroplet Release Using Photothermal Liquid Crystals

ToC figure



Supporting Information

Contactless Pulsed and Continuous Microdroplet Release Using Photothermal Liquid Crystals

*Pinar Beyazkilic, Samet Akcimen, Caglar Elbuken, Büilend Ortaç, Shengqiang Cai, and Emre Bukusoglu**

P. Beyazkilic, E. Bukusoglu

Department of Chemical Engineering

Middle East Technical University

Dumlupinar Bulvari No:1 Cankaya, Ankara 06800, Turkey

E-mail: emrebuk@metu.edu.tr

S. Akcimen, B. Ortaç, C. Elbuken

Institute of Materials Science Nanotechnology

National Nanotechnology Research Center (UNAM)

Bilkent University

Ankara 06800, Turkey

C. Elbuken

Faculty of Biochemistry and Molecular Medicine, Faculty of Medicine

University of Oulu

Oulu 90014, Finland

S. Cai

Department of Mechanical and Aerospace Engineering

Materials Science and Engineering Program

University of California, San Diego

La Jolla, California 92093, United States

IR spectrum of powder PDIB was recorded in attenuated total reflection mode of FTIR spectrometer. 1772 cm^{-1} band in FTIR spectrum revealed the formation of C=O stretching in the bis(oxalato) borate anion of PDIB dye (Figure S1). Atomic identification of PDIB was made using XPS. Bands at 532 eV and 198 eV in survey analysis showed the presence of O and B atoms, respectively and the band at 398 eV in the high-resolution N 1s spectrum revealed the formation of an imine (-N=C) bond (Figure S2).

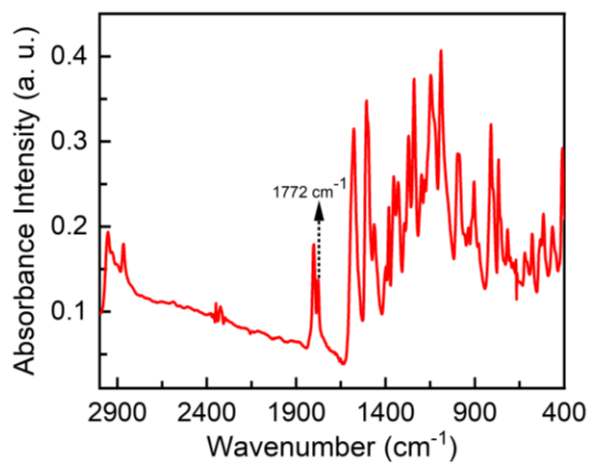


Figure S1. FTIR spectrum of PDIB dye.

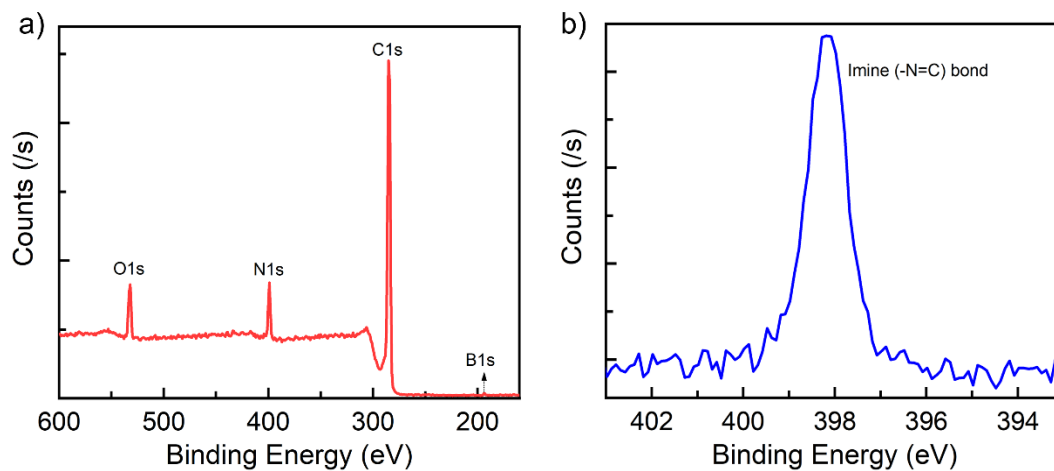


Figure S2. a) XPS analysis spectrum and b) high-resolution N 1s spectrum of PDIB dye.

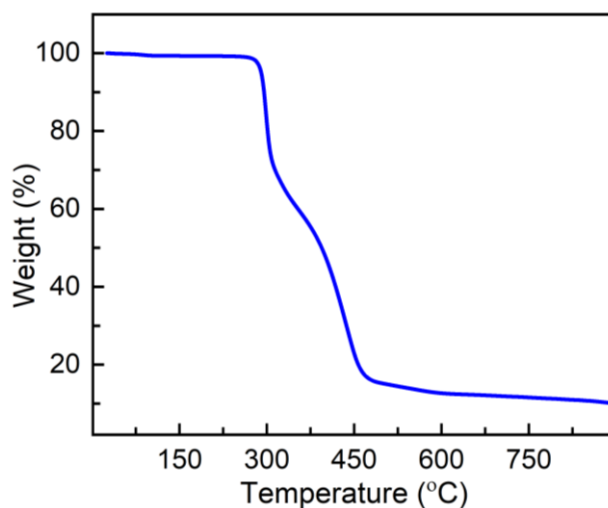


Figure S3. Thermogravimetric analysis spectrum of PDIB dye.

Table S1. Velocities of I-N border shift calculated for different PDIB percentage, laser beam spot size and power.

PDIB percentage [%]	Beam spot size [mm]	Laser power [mW]	I-N border shift velocity [mm s ⁻¹]
0.075	3	94	0.02
0.075	3	184	0.03
0.075	2	94	0.003
0.15	2	94	0.01

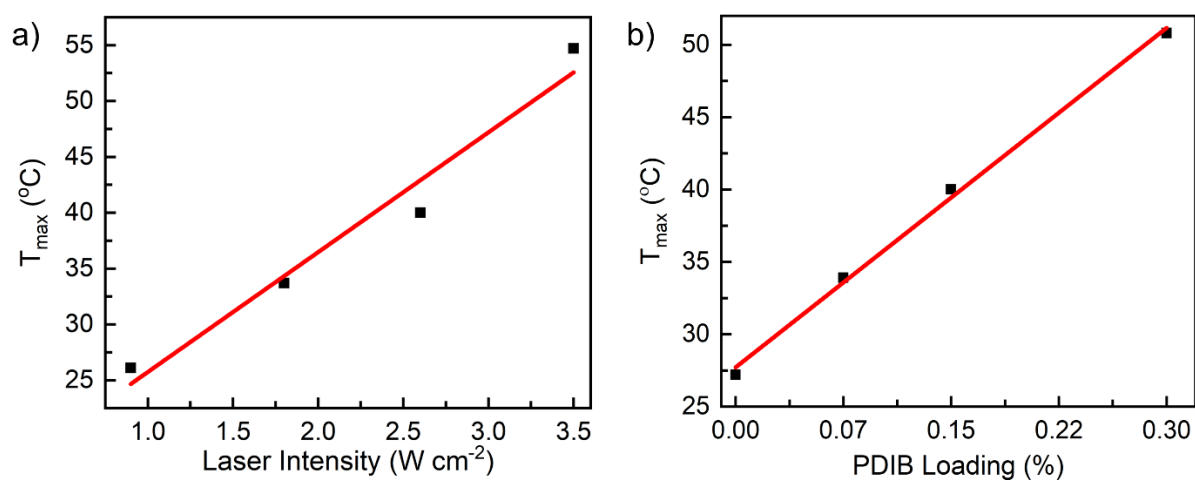


Figure S4. Maximum temperature values measured depending on the (a) laser intensity and (b) PDIB loading percentage.

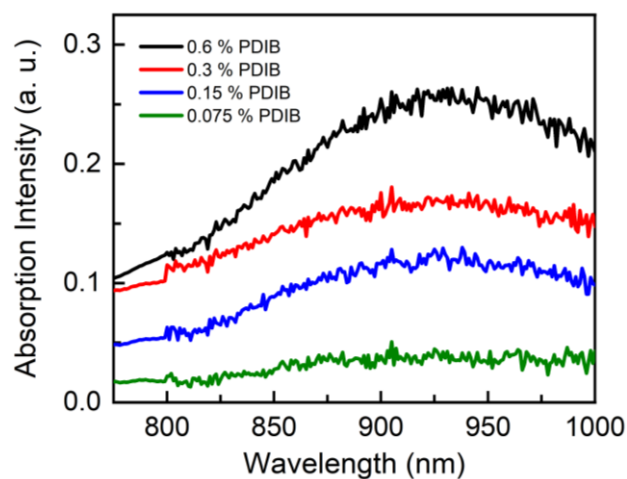


Figure S5. Absorption spectra of PDIB-LC hybrid films depending on the PDIB percentage.

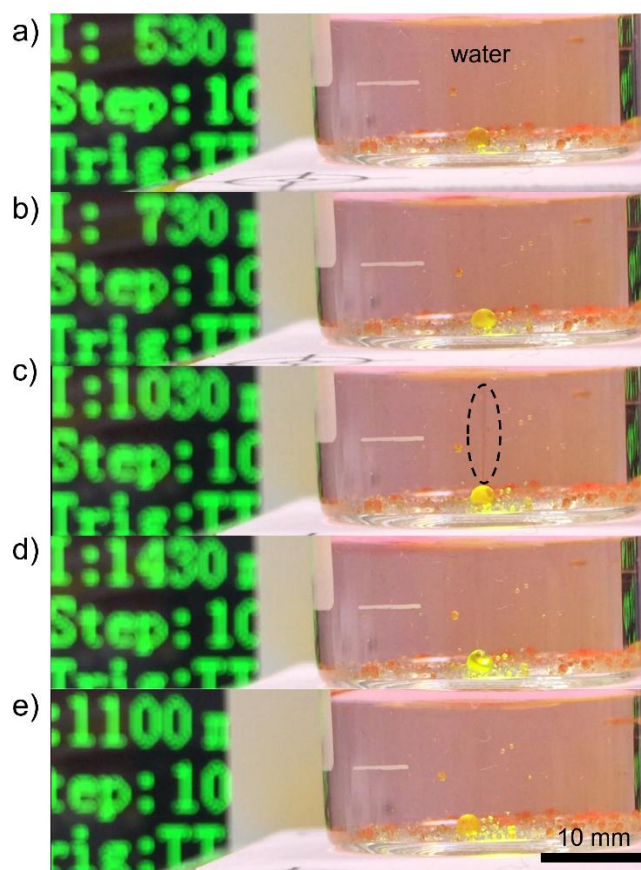


Figure S6. a) Excitation of droplet-shaped water-in-LC with a laser beam (1 mm-spot size) at an intensity of 23 W cm^{-2} (530 mA), b) 40 W cm^{-2} (730 mA), c) 70 W cm^{-2} (1030 mA), and d) 110 W cm^{-2} (1430 mA). e) Excitation of droplet-shaped LC with a laser beam (3 mm-spot size) at an intensity of $\sim 8 \text{ W cm}^{-2}$ (1100 mA). Dashed circle in (c) denotes the released dye.